

Article

Anticorrosion and Antibacterial Properties of Al NP–Epoxy Nanocomposite Coating on Grey Cast Iron

Marina Samardžija ^{1,*}, Marin Kurtela ², Marija Vuković Domanovac ³ and Vesna Alar ²

¹ Department of Chemistry, Faculty of Mining-Geology-Petroleum Engineering, University of Zagreb, 10110 Zagreb, Croatia

² Department of Welded Structures, Faculty of Mechanical Engineering and Naval Architecture, University of Zagreb, 10000 Zagreb, Croatia; marin.kurtela@fsb.unizg.hr (M.K.); vesna.alar@fsb.unizg.hr (V.A.)

³ Department of Industrial Ecology, Faculty of Chemical Engineering and Technology, University of Zagreb, 10000 Zagreb, Croatia; mvukovic@fkit.unizg.hr

* Correspondence: marina.samardzija@rgn.unizg.hr; Tel.: +385-1-5535-912

Abstract: In this study, different concentrations of aluminium nanoparticles (Al NP) were incorporated into epoxy resin and epoxy paint. Here, we present a detailed systematic study of different methods of incorporating inorganic nanoparticles into epoxy coating. This work aims to obtain an epoxy coating with anticorrosion and antibacterial properties. The physical properties of coatings such as thickness, hardness, colour, and adhesion did not change with the addition of nanoparticles. According to the SEM and EDS analyses, the distribution effect of Al NPs in epoxy coating was better with ultrasonic homogenisation than with mechanical stirring. The EIS and SECM measurements were used to investigate corrosion resistance. The coating with 1.0 wt.% Al NP showed the best physical and chemical properties. SECM examination indicated that nanoparticles in epoxy resin increase the protection efficiency by 25.75% and in the epoxy paint by 40.89%. The results also showed the antibacterial activity of aluminium nanoparticles by inhibiting the growth of biofilm-forming bacteria such as *P. aeruginosa* and *B. subtilis*.

Keywords: electrochemical corrosion; microbiologically corrosion; Al nanoparticles; mechanisms



Citation: Samardžija, M.; Kurtela, M.; Vuković Domanovac, M.; Alar, V. Anticorrosion and Antibacterial Properties of Al NP–Epoxy Nanocomposite Coating on Grey Cast Iron. *Coatings* **2023**, *13*, 898. <https://doi.org/10.3390/coatings13050898>

Academic Editor: Heping Li

Received: 18 April 2023

Revised: 4 May 2023

Accepted: 8 May 2023

Published: 10 May 2023



Copyright: © 2023 by the authors. Licensee MDPI, Basel, Switzerland. This article is an open access article distributed under the terms and conditions of the Creative Commons Attribution (CC BY) license (<https://creativecommons.org/licenses/by/4.0/>).

1. Introduction

Grey cast iron has been widely used in pipes serving as water mains [1] due to its good thermal conductivity, relatively low melting temperature, high damping capacity, and excellent castability [2]. Unfortunately, these properties deteriorate when metals interact with certain elements that recur within their environments, a process technically called corrosion [3]. Corrosion is the irreversible damage or destruction of a material and as such is a very expensive and dangerous phenomenon that causes serious problems in the world [4,5]. The National Association of Corrosion Engineers (NACE International) estimates global losses caused by corrosion at USD 2.5 trillion per year and the average annual cost of corrosion in the pipeline industry is estimated at USD 7 billion to monitor, replace, and maintain these assets [6,7]. The most conventional method for protecting metal structures against corrosion is to isolate the metal from corrosive agents [8]. Researchers are continuously seeking new innovative coatings with good corrosion resistance and high antibacterial activity [9]. Typically, municipal wastewater that flows through pipes is composed of multiple pathogens and non-pathogenic bacteria, organic/inorganic chemicals, suspended and dissolved compounds, and similar [10,11].

Microbiologically influenced corrosion (MIC) is a serious type of corrosion, as it accounts for approximately 20% of total economic losses [12]. The microbiological community that exists in wastewater is usually a combination of various types of bacteria, among which are pathogenic forms such as opportunistic pathogens (*Enterobacter cloacae*, *Enterococcus faecalis*, *Escherichia coli*, *Klebsiella pneumoniae*, *Proteus vulgaris* or *Pseudomonas aeruginosa*),

obligate pathogens from *Salmonella* and *Shigella* genera and enteropathogenic strains of *Escherichia coli*. It can also contain viruses, protozoa, fungi, flatworms, roundworms, and similar [13,14]. The rod-shaped Gram-negative aerobic bacteria *P. aeruginosa* prefer moist environments such as urban runoffs and sewage effluents [15]. Furthermore, these bacteria have a high potential for developing great resistance to a wide range of currently available antimicrobial agents [16]. Likewise, the Gram-positive aerobic bacteria *B. subtilis* are widely present in the environment and show a capability to deal with heavy metals and dyes in polluted waters [17]. The presence of an energy source, carbon source, redox mediators, and water are important factors for bacterial colonization of any surface. Then, the metabolic activities of these colonized bacteria influence the electrochemical reactions initiating MIC. Secretion of extracellular polymeric substances (EPS) and biofilm formation on the material surfaces are crucial steps that enhance the probability of metal corrosion and MIC [18].

Recently, with the development of nanotechnology [19], the term “nanocomposite” has appeared with at least one dimension on the nanometre scale [20]. Nanoparticles have been widely used as resin fillers to block micropores and improve the corrosion resistance and the mechanical properties of the resins due to their great surface-to-volume proportion with respect to conventional macroscopic materials [4]. The purpose of the study by Manjumeena and co-authors [21] was to obtain a nanocomposite with dual properties. According to their study, silver nanoparticles show great antibacterial properties due to their ability to release Ag^+ from nanoparticles which can damage the cell wall and cause oxidative stress. Talabi and co-authors [22] developed polymer nanocomposites with antibacterial properties. They showed that Cu^{2+} ions, which are released from copper nanoparticles, cause the denaturation of proteins in the bacterial membrane, by binding to DNA, which results in the cell not being able to replicate further. The surface-to-volume ratio of a nanoparticle is 35%–45% times higher as compared to large particles or atoms. This unique extrinsic property of the specific surface area of the nanoparticle is a contributory factor for its high value, and it also influences different intrinsic properties such as strong surface reactivity which is size dependent [23]. Due to all these properties of nanoparticles and the high viscosity of epoxy coating, it is hard to uniformly mix nano-size fillers into epoxy coating [15]. According to the available literature, there are different methods of incorporating nanoparticles into epoxy coating. In our last article, we employed strong mechanical stirring for the preparation of a nanocomposite of epoxy matrix and aluminium nanoparticles (Al NP) [24].

Pure aluminium is a metal that is soft, ductile, and corrosion-resistant [25]. Control over nano aluminium powder size has been crucial for changing properties. Slight changes in particle size can have a dramatic effect on surface area and therefore surface area-dependent properties such as rheology, powder mixing, dispersion, surface adsorption of condensed species, and bulk density [26]. Likewise, metal nanoparticles showed antibacterial behaviour against a wide series of bacteriological organisms [27]. Our interest is the development of a new anticorrosive and antibacterial nanocomposite coating to protect grey cast iron. The coating was fabricated with the addition of aluminium nanoparticles (Al NP) in a different ratio. In [24], the mechanical procedure for the preparation of the Al NP nanocomposite coating and its anticorrosive properties were demonstrated. In this paper, we investigated the influence of ultrasonic dispersion of Al NPs in an organic coating. Furthermore, in this study, we investigated the antibacterial properties of the metal powder of Al NPs. For all these purposes, we used electrochemical techniques (EIS and SECM), scanning electron microscopy (SEM), energy-dispersive X-ray spectroscopy (EDS) analyses, devices for establishing mechanical properties (Elcometer[®] 456, PosiTector[®] SHD, Elcometer 510) and bacteria (*P. aeruginosa* and *B. subtilis*) for the determination of antibacterial properties.

2. Materials and Methods

2.1. Materials

In this study, grey cast iron was investigated. The elemental composition of grey cast iron is shown in Table 1.

Table 1. The chemical composition of the grey cast iron.

Element	C	Si	Mn	P	S	Fe
Percent (%)	2.5	1.5	1.05	0.5	0.07	balance

Grey cast iron plates with dimensions of 9.5 cm × 0.9 cm × 15 cm were used as substrates. The surface of the grey cast iron was cleaned with abrasive blasting and ethanol (70 wt.%). Two epoxy coatings were used in the work. The first coating was prepared using pure epoxy resin (Bisphenol A, West System, UK) and hardener (polyamine, West System, UK) in a ratio of 3.5 to 1. The second coating was prepared using epoxy paint (Hempel, Croatia) and hardener (polyamine, Hempel, Croatia) in a ratio of 4 to 1. Aluminium nanoparticles (Al NP) with an average particle size of 100 nm were provided by Guangzhou Hongwu Material Technology Co., Ltd., Guangzhou, China.

2.2. Preparation of the Epoxy Coatings

The obtained Al NPs were used to prepare nanocomposites of Al NP–epoxy coating. In this method, different concentrations of Al NPs (0.50, 0.75, and 1.0 wt.%) were added to the epoxy solution. The procedure for the epoxy coating modified by Al NP is illustrated in Figure 1.

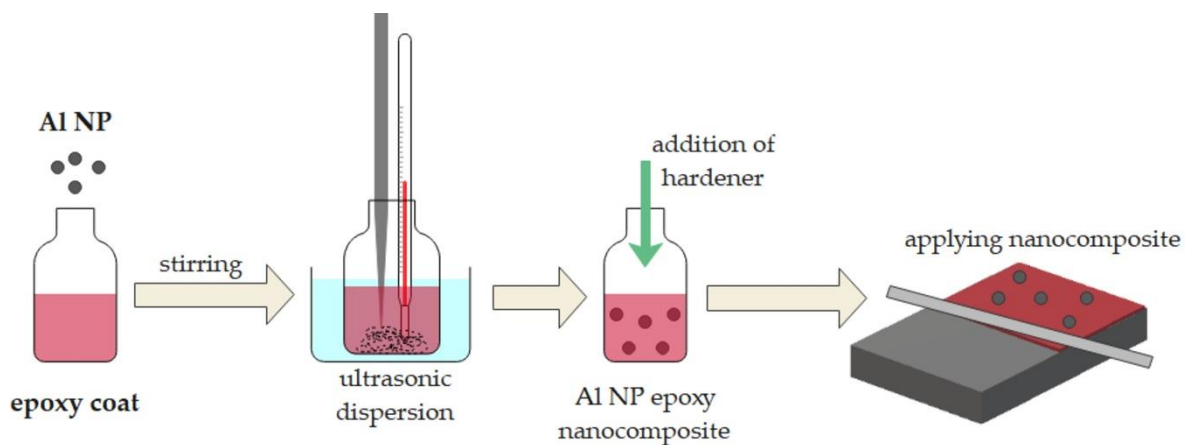


Figure 1. Preparation of the Al epoxy nanocomposite coating.

Al NPs were mixed with epoxy resin and epoxy paint (epoxy coating) using ultrasonic agitation for 20 min with a delay in the process due to the cooling of the nanocomposite. The hardener was added to the prepared samples and stirred until complete homogenisation. The obtained mixture was applied to the grey cast iron substrate using an applicator (150 µm). Then, the samples were dried under atmospheric conditions. After 24 h, another layer of nanocomposites was applied in the opposite direction (150 µm). The samples were left at room temperature (25 °C) for 7 days.

2.3. Coating Characterisation

The morphology of the Al NP samples was investigated by scanning electron microscope (SEM) (TESCAN Brno, Brno, Czech Republic). The size distribution and dispersion of nanoparticles, the homogeneity of the layer, and the occurrence of agglomeration were observed. The coated samples were also characterised using the energy-dispersive (EDS) detector.

Elcometer[®]456 (Elcometer Limited, Edge Lane, Manchester, UK) was used to assess the thickness of the nanocoating sample. Measurements were performed on ten different locations per sample. The change in the colour of the nanocomposite coating was determined using the RAL colour chart (RAL gGmbH, Siegburger, Germany). The hardness of the nanocomposite was tested according to ISO 868:2003 [28]. The testing was evaluated using PosiTector SHD Shore Hardness Durometer (DeFlesko Corporation, Ogdensburg, NY, USA). An adhesion test was performed to examine the effect of the coating strength of metal using an automatic Pull-Off Adhesion Tester (Elcometer 510, model T, Manchester, UK). The aluminium dollies (20 mm diameter) were glued on the Al NP nanocomposite using a two-part epoxy adhesive (Araldite resin and Araldite hardener). Complete curing of the adhesive was achieved by keeping the sample at 25 °C for 24 h.

The coating samples were exposed to the humidity chamber (Humidity Cabinet Model AB6), and the climatic chamber (Climatic chamber Kambic KK-190 CHLT, CiK Solutions GmbH, Karlsruhe, Germany). The humidity test was conducted according to EN ISO 6270-2 for five days [29]. To test the coating stability at low temperatures, the samples were placed in the climatic chamber for five days. The test cycle was set up in ten steps in which the temperatures changed from −5 °C, with 0% humidity, to 10 °C, with 70% humidity. The samples were left at each temperature for 8 h. The accelerated testing was performed on two samples per coating. After the humidity test, and the icing/deicing process, the physical properties of the samples were tested after they reached room temperature.

The corrosion protection performance of the epoxy coating and Al NP–epoxy nanocomposite were studied in 3.5 wt.% NaCl solution by EIS (VersaSTAT 3, AMETEK Scientific 131 Instruments, Princeton applied research, Berwyn, PA, USA). Open-circuit potential (OCP) was first obtained over a period of 20 min to study the changes in the corrosion potential of the coatings. The electrochemical cell consisted of a graphite rod as the auxiliary electrode, a saturated calomel electrode as the reference, and the epoxy coating and/or Al NP–epoxy nanocomposite specimen as the working electrode. The frequency range of 0.1 to 10⁵ Hz with an amplitude of 10 mV was used. The impedance data were fitted using the ZSimpWin software. The Intermittent Contact-Scanning Electrochemical Microscopy (ic-ac-SECM) (M470, BioLogic, France) test of epoxy resin, epoxy paint, and epoxy nanocomposite with 1% of Al NP was used to observe real impedance distribution over a certain area. The 3DIsoPlot program was used to obtain the topography of the samples in 3D view. A three-electrode system, immersed in tap water, was above the surface of the nanocomposite. This three-electrode system consisted of the Ag/AgCl/KCl (saturated) reference electrode, the platinum sheet as the counter electrode, and of the UltraMicroElectrode (UME) probe for measuring the local electrochemical activity. The UME probe with 10 µm diameter platinum wire was used.

Pseudomonas aeruginosa and *Bacillus subtilis* were taken as the test bacteria. The antibacterial activity of the Al NP was performed using the well-diffusion method [30]. The final densities of the bacterial suspensions' cells were about 10⁸ and 10⁷ CFU/mL, respectively. The bacterial culture was inoculated from fresh colonies on agar plates into 20 mL Muller Hinton culture medium. The nanoparticle samples dissolved in distilled water (100 µg/mL) were added from the stock into each well. The zone of inhibition was measured using a ruler. After 24 h, the appearance of the inhibition zone was observed.

3. Results and Discussion

3.1. Characterisation of Al NP

The SEM microstructure of Al NPs is shown in Figure 2a. The surface of nanoparticles is a fluffy powder with spherical properties. To determine the composition of Al NP, the EDS analysis was carried out.

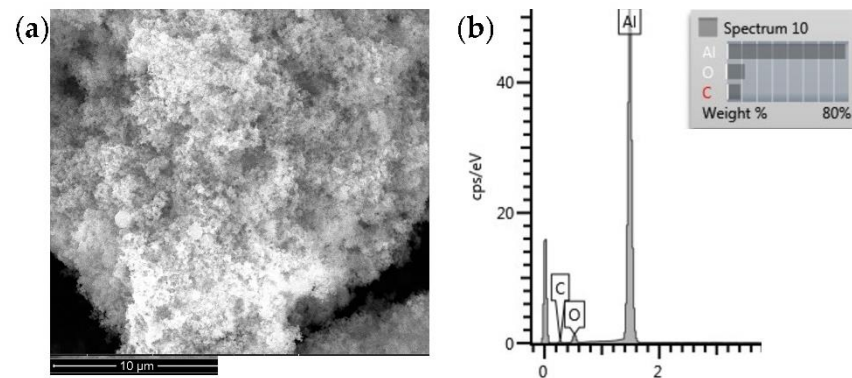


Figure 2. SEM image (a) and EDS profile (b) of pure Al NP.

The EDS analysis of Al NPs (Figure 2b) determined the mass fraction of the aluminium nanoparticles of about 80%. Spectrum minor elements such as O and C were due to contamination.

3.2. Evaluation of Mechanical Properties

Epoxy paint and epoxy paint nanocomposites with 0.50%, 0.75%, and 1.0% of Al NP were exposed to the humidity (ISO 6270-2) and climatic chambers. According to ISO 12944-6, nanocomposites were classified as corrosivity category C4 and durability up to 15 years [31]. After exposure of the samples to the corrosive media, mechanical properties were observed (Table 2).

Table 2. Results of changing thickness, hardness, adhesion force, and colours of epoxy paint and nanocomposite paint samples in different corrosion conditions.

	Samples	Epoxy Paint	0.5%_Al	0.75%_Al	1.0%_Al
thickness, μm	unexposed	249.9	278	256.4	275.5
	humidity chamber	275.9	263	263.2	285.6
	climatic chamber	248.8	259.9	271	292.3
Hardness, Shore D	unexposed	83.4	83.8	82.8	82.0
	humidity chamber	83.2	80.3	80.0	80.2
	climatic chamber	81.0	83.0	81.4	81.8
adhesion, MPa	unexposed	8.34 8.31	9.59 9.42	12.10 10.30	13.47 14.18
	humidity chamber	9.85 10.20	10.87 11.52	11.89 12.56	13.24 12.12
	climatic chamber	10.11 10.52	16.57 13.56	13.15 13.16	12.43 11.41
RAL colours	unexposed	3013	8015	8016	8017
	humidity chamber	3013	8015	8016	8017
	climatic chamber	3013	8015	8016	8017

According to Table 2, it is evident that there was no change in the thickness and hardness of the coating on the samples despite the addition of Al NPs and the exposure of the coating to corrosive conditions. The adhesion of the coating to the metal substrate showed a small increase with the addition of Al NPs. The results showed that the direct addition of Al NPs to the epoxy paint reduced the stress in the coating. The particle effect, the uniform dispersion of the filler in the epoxy paint, and the strength of the bond with the paint contribute to a better stress transfer. The strengthening mechanism was due to

the tight bond between the nanoparticles and the epoxy paint, which can limit the mobility of the polymer chains [32]. Samples that were exposed to the humid and air-conditioned chambers showed a smaller increase in adhesion. An increase in the adhesion force could be caused by increasing or decreasing temperature and moisture in the humidity and climatic chambers. As shown in the paper, the addition of Al NPs to the epoxy matrix significantly changed the colour of the coating [24].

3.3. Evaluation of Anticorrosion Properties

The impedance data were analysed using the equivalent electrical circuits (EEC) shown in Figure 3. The model's outer and inner circles corresponded to the high and low-frequency loops, respectively. Indeed, the outer circle was used to characterise the coating properties. The inner circle of EEC with two-time constants, was the feature of the double layer formed at the coating/metal interface [33]. Figure 3 shows that the first resistance encountered by the alternating current was the electrolyte resistance, R_s , which had a negligibly small value. The coating resistance, R_{coat} , provided another resistance to the passage of current. At the phase boundary between solid and liquid, an electrical double layer appeared, representing the capacity of the coating, CPE_{coat} . After a long time of exposure of the coating to an aggressive medium, damage occurred to the epoxy paint and thus the electrolyte could more easily reach the surface of the grey cast iron the alternating current encountered a charge transfer resistance, R_{ct} , which also had its capacity, CPE_{dl} [34].

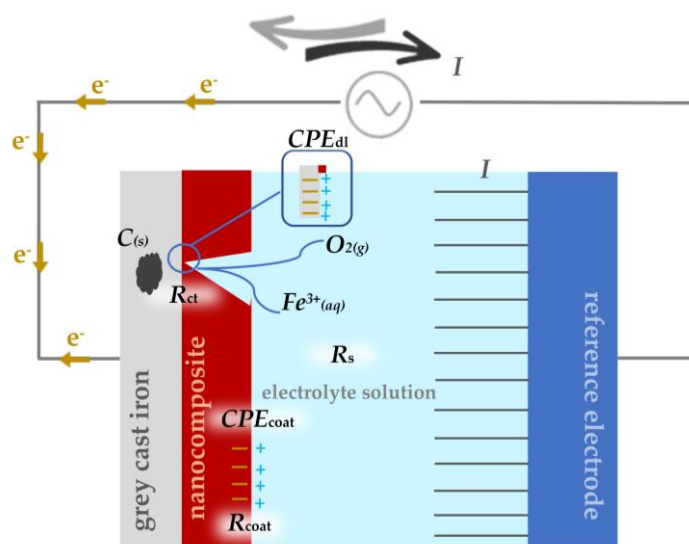


Figure 3. The equivalent electrical circuits used for describing the impedance response of epoxy coating and nanocomposite with 0.5, 0.75, and 1.0% Al NP.

Figure 3 shows the electrochemical mechanism of corrosion destruction on the surface of grey cast iron, which is called graphitization. When the aggressive medium reaches the surface of grey cast iron, it will initiate the anodic dissolution of iron by leaving free graphite [35]. To slow down this process, the epoxy resin and the epoxy paint were modified with Al NPs, and tests were performed in a 3.5 wt.% NaCl solution using alternating current.

The EIS results for the epoxy paint and nanocomposite samples with different concentrations of Al NPs (0.50, 0.75, 1.0%) were presented in Nyquist and Bode diagrams (Figure 4a,b). The measurement was made immediately after immersion in 3.5 wt.% NaCl solution. The results showed coating resistance, R_{coat} , which reflected the anti-penetrating ability of the coating to electrolyte solution [36]. All samples showed a single capacitive loop, meaning that there was no electrolyte penetration. Pure epoxy showed a lower coating resistance value, while the samples with 0.50 and 0.75% Al NPs had slightly higher resistances. The increase in resistance was significantly more pronounced in the sample containing 1.0% Al NPs. Nanoparticles embedded in the coating resisted the passage

of current and provided high resistance. The large resistance values in the Nyquist plot were confirmed by the Bode phase angle in Figure 4b. The Bode phase angle plots were further analysed to explain the effectiveness of the coating. All tested samples achieved a constant phase angle value extending from the medium frequency range (100 Hz) to the high frequency range (10^5 Hz) during the entire exposure time, which indicated that the coating had not started to degrade. In the case of short-term immersion in the electrolyte, the properties of the protective coating remained intact.

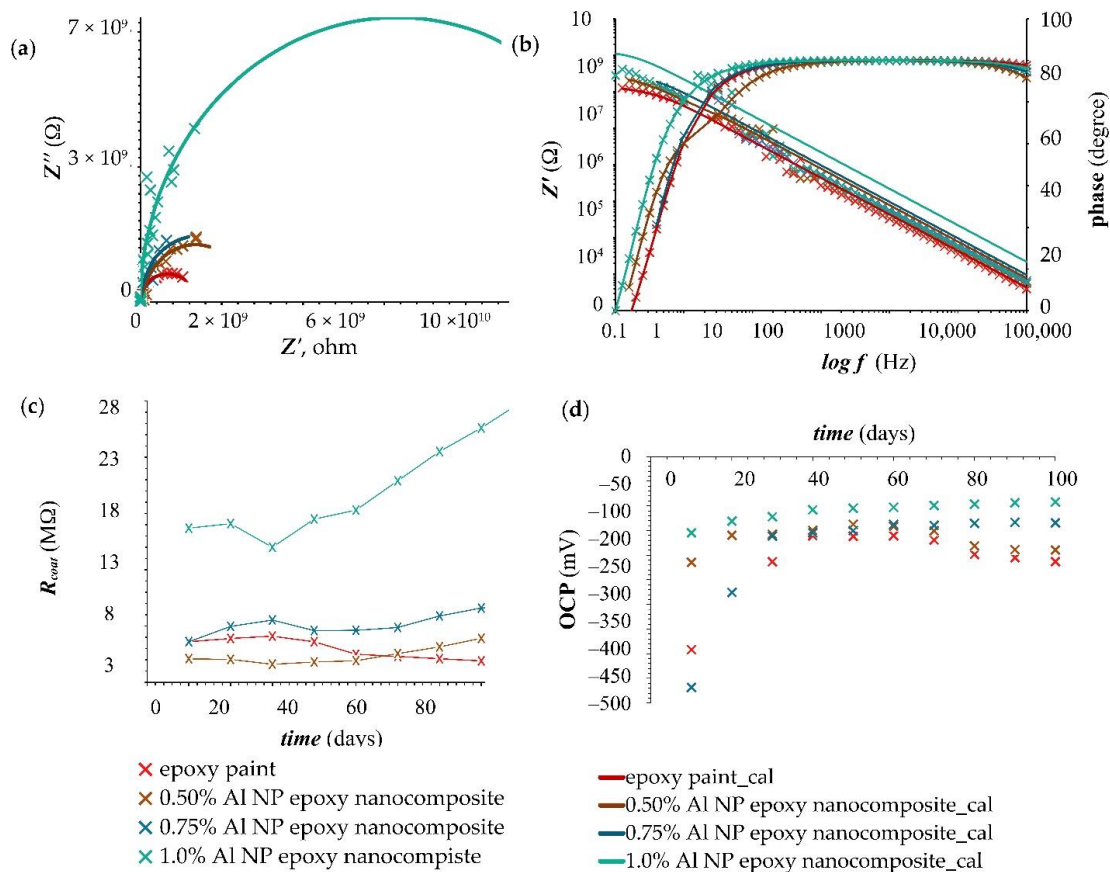


Figure 4. Nyquist and Bode plots of (a,b) epoxy paint and epoxy paint with different concentrations of Al NP immediately immersed in 3.5 wt.% NaCl solution. Corrosion resistance values (c) for samples in 3.5 wt.% NaCl solution during a 100-day immersion. Variations of OCP values (d) for samples during a 100-day immersion.

The value of R_{coat} for the blank epoxy coating (paint) without nanoparticles and for the coatings with different concentrations (0.50, 0.75, and 1.0%) of Al NP in the epoxy paint at different interval times over a 100-day immersion in 3.5 wt.% NaCl solution is shown in Figure 4c,d.

After 10 days, the epoxy paint showed the same resistance as the nanocomposite sample with 0.75% Al NPs. With a longer exposure time (after 50 days), the resistance of the blank epoxy gradually began to decrease (Figure 4c). Constant resistance values in all nanocomposite samples were maintained for 50 days, after which there was a slight increase in resistance in samples with 0.50% and 0.75% Al NPs, while the sample with 1.0% Al NPs showed a larger increase (Figure 4c). The obtained results indicated that it took 50 days to form an oxide film in the epoxy paint. The higher the concentration of nanoparticles, the greater the formation of the oxide film and the better the coating protection. Figure 4c shows that the highest resistance was achieved with the nanocomposite sample containing 1.0% Al NPs. This sample showed the highest resistance immediately at the beginning of the measurement. The increase in corrosion resistance could be attributed to a higher

concentration of nanoparticles that created better adhesion and compatibility with the epoxy matrix, reduced the transport paths for the passage of corrosive electrolyte through the system coating, led to a decrease in the capacitance of the coating, and reduced corrosion reactions [16,30].

Open-circuit potential (OCP) is the potential of a working electrode when no current is applied to the cell [37]. In Figure 4d, all samples showed a constant OCP value after 50 days. After 100 days of exposure to an aggressive medium, the epoxy paint showed the highest negative potential value, which indicated weaker protective properties. Nanocomposites showed a more positive potential value that balanced out after 50 days indicating the beginning of the formation of a protective oxidative film. The values of the parameters shown on the equivalent circuit are listed in Table 3.

Table 3. EIS parameters values after fitting with equivalent circuit for epoxy paint and epoxy paint with different concentrations of Al NPs immediately immersed in 3.5 wt.% NaCl solution.

Parameters	Epoxy Paint	0.50% Al NP-Epoxy Nanocomposite	0.75% Al NP-Epoxy Nanocomposite	1.0% Al NP-Epoxy Nanocomposite
R_s, Ω	479.0	495.0	481.0	313.4
R_{coat}, Ω	$1.78 \cdot 10^8$	$1.80 \cdot 10^9$	$1.93 \cdot 10^9$	$1.87 \cdot 10^{10}$
$CPE_{coat}, S \cdot sec^n$	$4.22 \cdot 10^{-9}$	$1.47 \cdot 10^{-10}$	$2.60 \cdot 10^{-10}$	$2.76 \cdot 10^{-11}$
n	1	1	1	1
R_{ct}, Ω	$1.17 \cdot 10^9$	$8.38 \cdot 10^8$	$1.30 \cdot 10^9$	$2.87 \cdot 10^9$
$CPE_{dl}, S \cdot sec^n$	$3.65 \cdot 10^{-10}$	$2.05 \cdot 10^{-10}$	$3.01 \cdot 10^{-9}$	$7.22 \cdot 10^{-11}$
n	1	1	0.84	0.8

Considering the results reported in Table 3, CPE is a constant phase element of the double layer showing its capacitive properties, which depend on the empirical constant n . The CPE_{coat} value of the nanocomposite decreased by adding nanoparticles to the epoxy paint. The lower value of CPE_{coat} indicates superior corrosion resistance due to low electron storage.

To detect the presence of the aluminium oxide film, EDS microanalysis was performed at a point on the surface of the powder sample obtained by the reaction between Al NPs and distilled water (Figure 5).

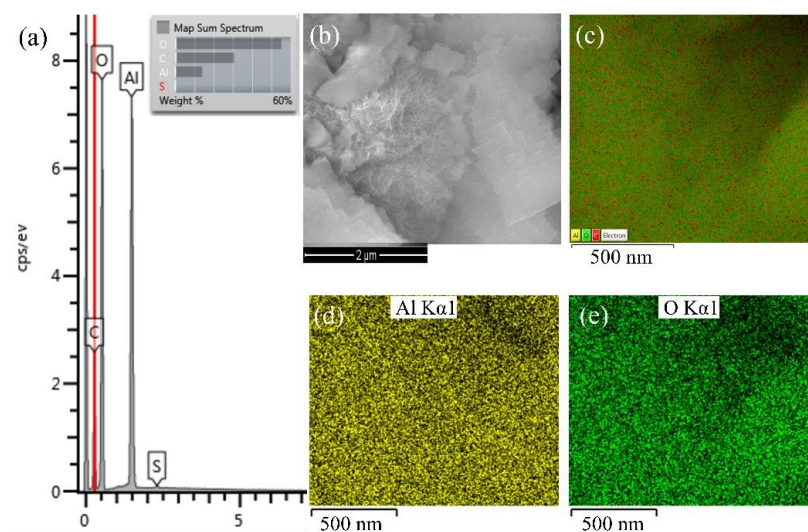


Figure 5. Results of (a) Surface spectrum, (b) SEM image, (c) collective colouring of surface maps of prepared aluminium oxide particles and partially coloured maps of the distribution of individual chemical elements in aluminium oxide particles: (d) Al K series, and (e) O K series.

Observing the size of the formed particles, an increase in the volume of the particles was visible in Figure 5a. The display of partial colours for aluminium and oxygen elements indicated that aluminium oxidation had occurred (Figure 5b,c). The EDS analysis cannot detect the presence of hydrogen in the compound, so according to the literature, the reactions that occur at the interface between Al NPs and a neutral aqueous medium are shown in Figure 6 [38].

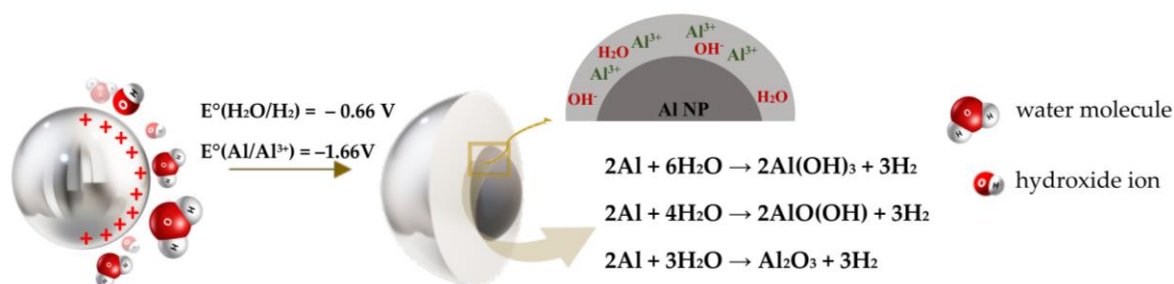


Figure 6. Mechanism of aluminium nanoparticle oxidation.

The oxidation process of a metal nanoparticle included two mechanisms, as shown in Figure 6. A nanoparticle in contact with an aqueous medium became electrically positively charged and, using van der Waals interactions, began to attract OH^- ions and the negative polar part of the H_2O molecule. After physical adsorption, due to the existence of a driving force (potential difference), Al NP oxidation and H_2O reduction occurred. The resulting oxidized products together with the metal surface created a chemisorbed monolayer [39,40]. The aqueous solution was a weak electrolyte, which means that it consisted more of water molecules than ions, and thus the formed aluminium ions could react with water molecules (H_2O) and form hydroxide ions (OH^-) [38]. According to the literature, the first possible reaction product is $\text{Al}(\text{OH})_3$ (bayerite). The second possible reaction product is $\text{AlO}(\text{OH})$ (boehmite). The third possible reaction product is Al_2O_3 (alumina). These reactions are all thermodynamically favourable over a wide temperature range from room temperature to temperatures far above the melting point of aluminium (660°C). In addition, all these reactions are highly exothermic [41]. The outer layer consisted of a mixture of Al_2O_3 and a hydrated layer, mostly in the form of amorphous $\text{Al}(\text{OH})_3$, while the inner part was mostly made of Al_2O_3 and a small amount of aluminium oxyhydroxide in the form of $\text{AlO}(\text{OH})$. Such a coating (Al_2O_3 - $\text{AlO}(\text{OH})$) was characterised by continuity and resistance to certain electrolytes ($3.91 < \text{pH} < 8.64$) [39]. The layers may have different thicknesses and chemical compositions depending on the methods used for the production and passivation of the powders [42]. The oxide layer thickness remained stable for at least 30 days, showing that the native oxide acted as a passivation layer preventing further oxidation [43]. Consolidation of inorganic fillers into the polymeric coating formulation can diminish porosity and draw out the lifetime of the composite coating [44].

The appearance of a protective oxidative film on the surface of nanoparticles led to an increase in corrosion resistance. The mechanism of formation, the connection of Al NPs with epoxy paint, and the degradation of Al NPs in epoxy paint are shown in Figure 7.

According to literature data [26,45,46], by adding a hardener, the aliphatic amine started hardening by nucleophilic attack of the amine group on the epoxy ring of the monomer (Figure 7). At the same time, the nanoparticle could react with both the hardener and the epoxy paint due to its small size. When the epoxy ring was opened, the hydroxyl groups that serve as bonding sites became strong electromagnetic bonds between the epoxy and the metal molecules. At the beginning of exposure to an aggressive medium, the nanoparticles were well embedded in the epoxy paint, which protected them from rapid oxidation. To prevent the oxidation of Al NPs, layers of organic and inorganic coatings could be applied to their surface [42]. The protective barrier properties of the epoxy paint decreased over time. Organic polymeric coatings mostly protect against corrosion by forming a barrier to disengage the metal from the surrounding environment. Nonetheless,

all polymeric coatings are porous to destructive species, for example, oxygen, water, and chloride particles [44]. The used aluminium nanoparticles in contact with the aqueous medium formed an aluminium oxide and smaller amounts of aluminium hydroxide and oxyhydroxide. Due to good dispersion, and interfacial compatibility of composites, a “maze effect” can be formed to prevent the penetration of corrosive media, prolong the penetration path of corrosive media in the coating, and ultimately delay the occurrence of corrosion [47]. This whole mechanism of protection of grey cast iron relied on a cathodic passivation process in which the aluminium in the coating acted as the sacrificial anode and protected the iron. According to the obtained EIS data (Figure 4c), an aluminium oxide film was formed after the sample had been immersed in an aggressive medium for 50 days. As a result, we can conclude that as the aggressive medium started to diffuse through the epoxy coating, more and more nanoparticles were completely and/or partially oxidized and the corrosion resistance increased (Figure 6).

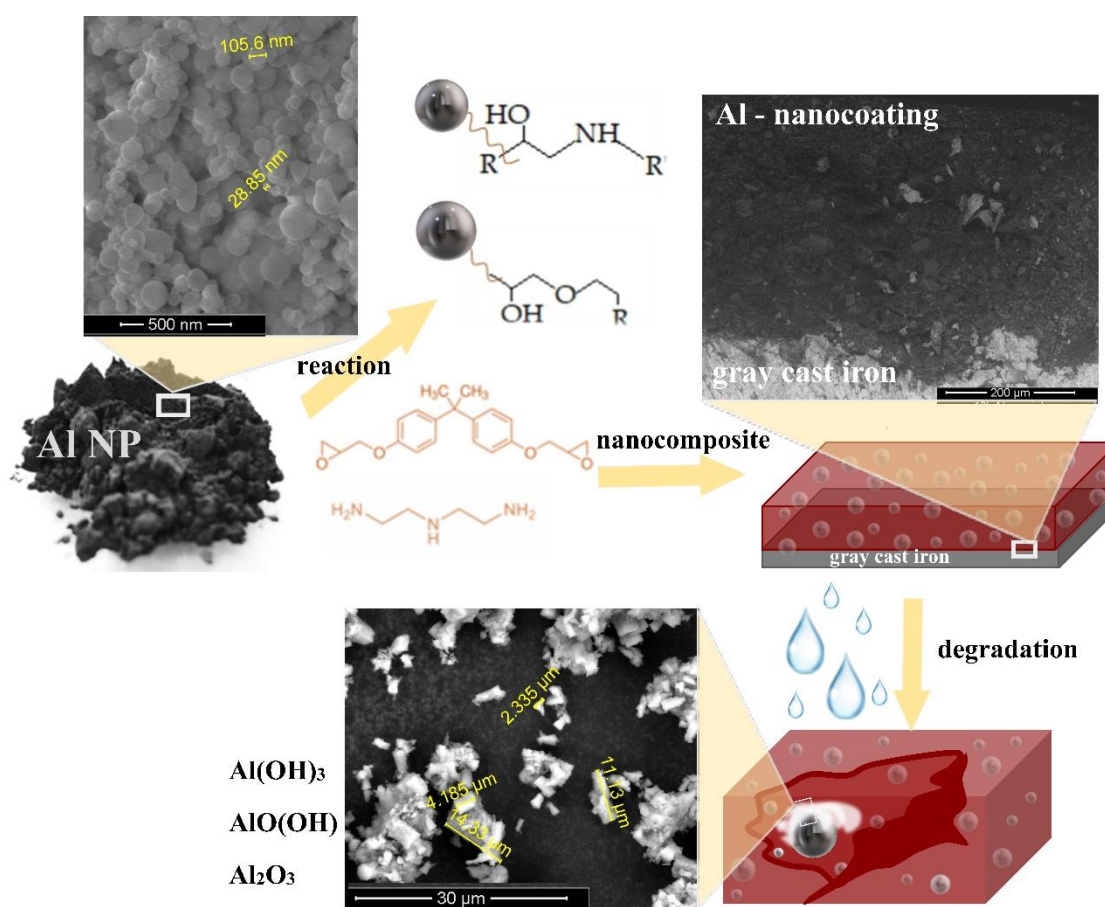


Figure 7. The mechanism of nanoparticle interaction with the epoxy paint and hardener, the degradation of the nanocomposite, and the formation of an oxidation film on the Al NP.

3.4. Surface Characterisation of 1.0% Al NP–Epoxy Nanocomposite

3.4.1. SEM/EDS Analysis

As 1.0% Al NP–epoxy nanocomposite was found to be the formulation with the best anticorrosion properties, the surface of the same sample was tested. The cross-sectional SEM image of the nanocomposite with 1.0% Al NPs prepared in epoxy paint is shown in Figure 8a,b.

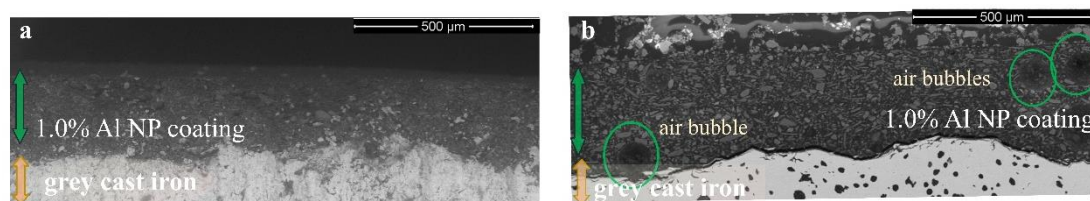


Figure 8. SEM cross-sectional morphology of nanocomposite with 1% Al NP prepared using (a) ultrasonic homogeniser and (b) mechanical mixing.

Figure 8 shows the result of two methods of preparing a nanocomposite containing 1.0% Al NPs. The preparation of the nanocomposite using ultrasonic mixing is shown in Figure 8a, while Figure 8b shows the nanocomposite prepared using a mechanical mixer. The results of mechanical mixing were published in the paper [24] and showed that the anticorrosive properties of the coating had improved in a short period of time. The reason for the short application of this nanocomposite was the appearance of air bubbles, as shown in Figure 8b. By applying ultrasonic mixing, better anticorrosive properties were achieved over a longer period. Figure 8a shows a cross-section of the nanocomposite, without air bubbles. Table 4 shows the advantages and disadvantages of both methods for the preparation of the nanocomposite material.

Table 4. Advantages and disadvantages of using mechanical and ultrasonic mixing in the preparation of nanocomposite coating.

	+	–
Mechanical stirring	Faster preparation of the sample It is not necessary to cool the Sample quiet mode of operation	Complicated handling of the device Complicated cleaning of the mechanical mixer The appearance of trapped air bubbles The appearance of nanoparticle agglomerates at higher concentrations
Ultrasonic stirring	Easy handling of the device Simple probe cleaning Easy air removal Better dispersion of nanoparticles	Heating the sample Longer sample preparation As the viscosity decreases, the device makes more noise

Better corrosion resistance and stability of the sample were obtained by ultrasonic preparation of nanocomposites due to better dispersion of nanoparticles and the absence of air bubbles. During sample preparation, air bubbles were released due to the heating of the coating. As the viscosity of the liquid decreased with the increase in temperature, air bubbles were released more easily. A risk of degradation of the base polymer, however, existed during processing [48]. To avoid this unwanted process, the epoxy paint must be heated to the temperature recommended by the manufacturer. Loss of solvent from the nanocomposite during preparation did not affect the reduction of anticorrosive properties.

Figure 9a shows the EDS spectra and chemical composition of the cross-section of the nanocomposite with 1% Al NP, which was prepared using an ultrasonic homogeniser in epoxy paint. SEM analysis of the sample is shown in Figure 9b. Figure 9d,e show the EDS distribution map of aluminium and oxygen in the cross-section of the nanocomposite with 1% Al NPs. The incorporation of Al NPs showed a uniform and homogeneous distribution in the entire measurement area of the nanocomposite cross-section. Additionally, according to the partial staining, we see that there was no formation of aluminium agglomerates. In the pure epoxy resin, as shown by the EDS analysis in Figure 10, the Al NPs were evenly distributed and remained at the nanoscale, which confirms that the nanoparticles did not start to form agglomerates.

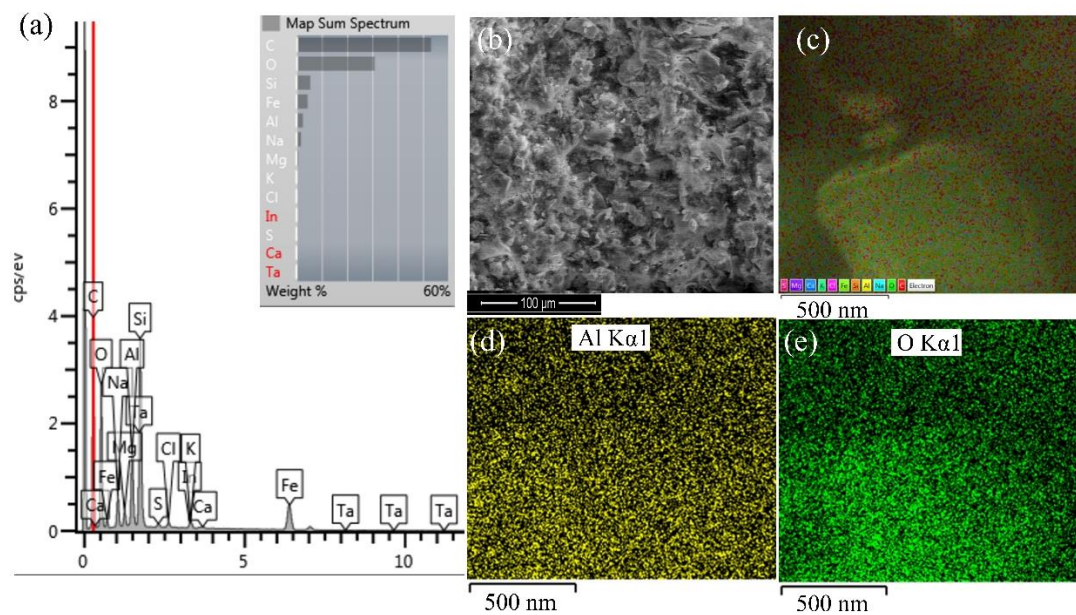


Figure 9. Results of (a) cross-sectional spectrum of the sample surface (b) SEM image of the sample surface (c) EDS cross-section map, and distribution of (d) aluminium and (e) oxygen in 1% Al NP-epoxy paint nanocomposite coating.

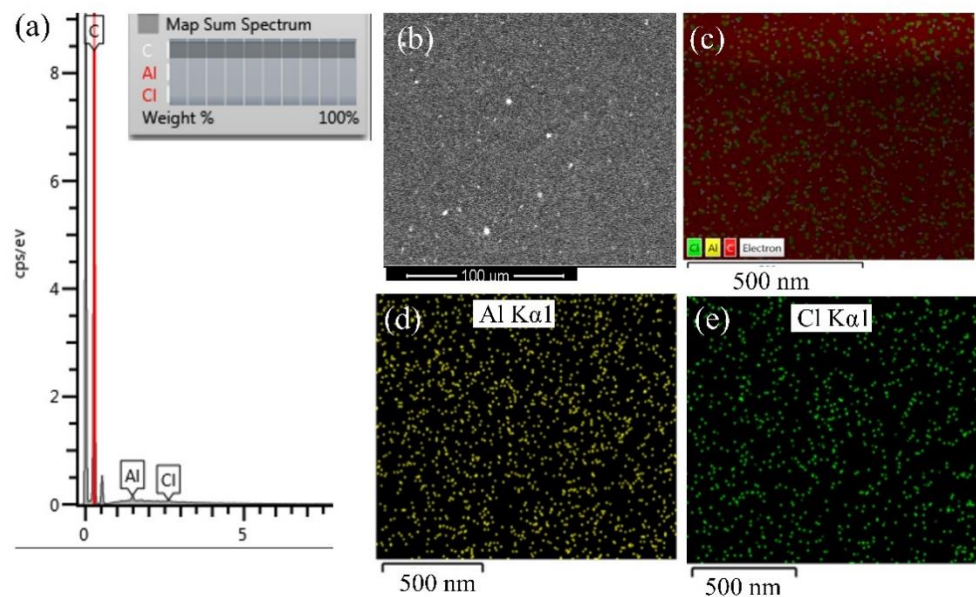


Figure 10. Results of (a) cross-sectional spectrum of the sample surface (b) SEM image of the sample surface (c) EDS cross-section map, and distribution of (d) aluminium and (e) chlorine in 1% Al NP-epoxy resin coating.

3.4.2. ic-ac-SECM Analysis

SECM provides electrochemical activity and topographic information about the surface reactions at the micrometre scale in aqueous environments [49]. We used this technique for the characterisation of the influence of the nanoparticles in the epoxy resin and epoxy paint. In the first experiment, it was necessary to find the appropriate vibration frequency so that the ultramicroelectrode (UME) could react with the surface (Figure 11). The piezo sensor was used to determine the distance of the UME from the surface of the sample. During the AC characterisation, the frequency applied to the piezo was automatically swept up to 600 Hz and the signal gain was recorded. The amplitude was 0.1.

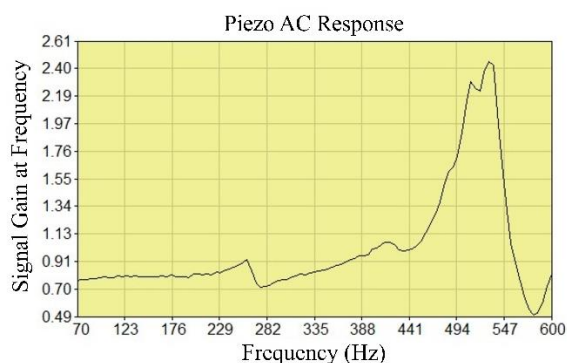


Figure 11. Determination of the vibration frequency of the UME.

The real impedance measured was the result of the surface activity and constant distance between the UME and the sample surface. The measurements were performed in tap water (Figure 11). The topography of the surface was determined on samples that did not contain nanoparticles and on samples obtained by ultrasonic mixing of epoxy resin and epoxy paint with 1.0% Al NPs.

The distribution of real impedance resistance values on the surface of pure epoxy resin, epoxy paint, 1.0% Al NP–epoxy resin, and 1.0% Al NP–epoxy paint nanocomposite coating is shown in Figure 12. The UME that recorded the topography moved along the *x*-axis from 0 to 0.5 mm, the *y*-axis from $-0.25 \mu\text{m}$ to $0.25 \mu\text{m}$, and the *z*-axis was set to the constant distance determined by the piezo sensor.

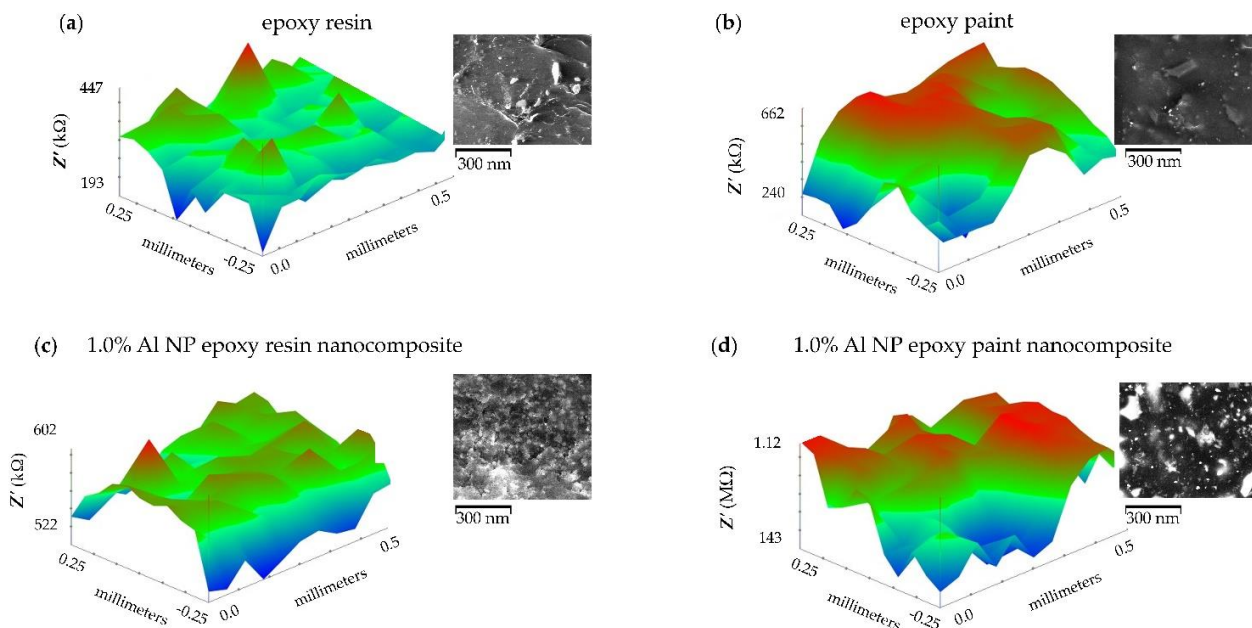


Figure 12. ic-ac-SECM distribution of real impedance per surface for samples: (a) epoxy resin, (b) epoxy paint, (c) 1.0% Al NP–epoxy resin nanocomposite, (d) 1.0% Al NP–epoxy paint nanocomposite coating immersed in tap water.

There is a small variation in the measured values of the impedance (from 522 to 602 kOhms) of the epoxy resin indicating a homogeneous structure (Figure 12a). A larger difference in real impedance distribution was observed in the epoxy paint sample (Figure 12b). The occurrence of localised peaks was surrounded by boundaries of higher impedance. The reason for the increase could be interpreted as the result of the effect of added coating components, such as additives in the epoxy paint. In the case of the sample containing 1.0% Al NPs in the epoxy resin, the impedance distribution was uniform, which resulted in

a homogeneous structure (Figure 12c). The sample containing 1.0% Al NPs in the epoxy paint showed the greatest resistance but also a large distribution of resistance (Figure 12d). A deviation in the impedance resistance values appeared due to the densely distributed aluminium nanoparticles located right next to the surface and inside the coating itself. The aluminium particles, located right next to the surface, reacted with the UME and allowed the current to flow, thus increasing the value of the current. Particles that were further from the surface were not able to have a complete impact on the UME, but the epoxy resin came to the fore, and the current flow decreased.

The obtained values which are shown in Figure 12 for coating resistance were used to calculate the nanocomposite protection efficiency (CPE) using the following equation [24]:

$$CPE = \frac{Z'_{coatwithAlNP} - Z'_{coatwithoutAlNP}}{Z'_{coatwithAlNP}} \quad (1)$$

The calculated nanocomposite efficiency obtained by ic-ac-SECM measurement of epoxy, epoxy paint, 1.0% Al NP–epoxy resin nanocomposite, and 1.0% Al NP–epoxy paint nanocomposite coating immersed in tap water, is shown in Table 5.

Table 5. Calculated coating protection efficiency (CPE, %) for non-modified and modified epoxy coating immersed in tap water.

Samples	Epoxy Resin	1.0% Al NP–Epoxy Resin Nanocomposite	Epoxy Paint	1.0% Al NP–Epoxy Paint Nanocomposite
Z'_{max} (k Ω)	447	602	662	1120
CPE (%)	-	25.75	-	40.89

Nanoparticles in pure epoxy resin increase the protection efficiency by 25.75% and in the epoxy paint by 40.89%.

3.5. Evaluation of Antibacterial Properties

To develop a nanocoating with antibacterial properties, we investigated the antibacterial activity of Al NPs. Inorganic nanoparticles with antimicrobial activity are emerging as a new class of additives to coating materials to fulfil the increasing general demands for achieving dual properties of nanocomposites [21]. In the literature, there is almost no data on the toxicity of pure Al NPs, most of the literature studies aluminium oxide nanoparticles (alumina).

The antibacterial activity of Al NP nanoparticles against *P. aeruginosa* (Gram-negative) and *B. subtilis* (Gram-positive) was measured using the well-diffusion method (Figure 13a,b).

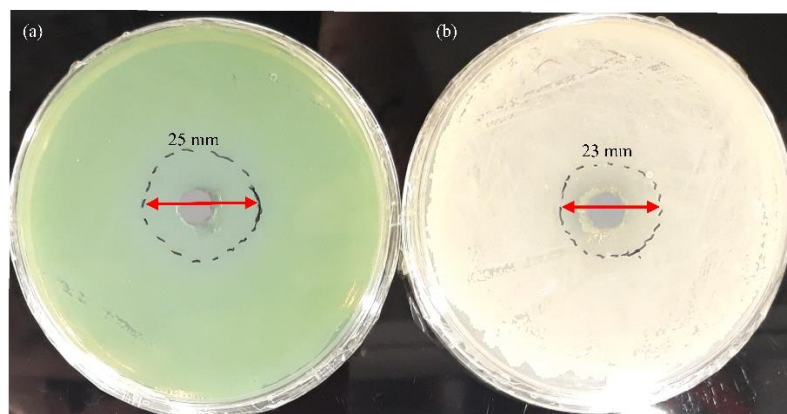


Figure 13. Antibacterial activity of pure Al NPs. Zone of inhibition of Al NP against (a) *P. aeruginosa* and (b) *B. subtilis* after 24 h.

The inhibition zone diameter indicated that Al NPs had a great antimicrobial effect (Figure 13a,b). Pure Al NPs produced zones of inhibition of 25 mm against *P. aeruginosa* and 23 mm against *B. subtilis*. In general, differences in the cell wall structure between Gram-positive and Gram-negative bacteria could affect the interaction between NPs and bacteria. Gram-positive bacteria had a thick outer cell wall formed by a thick peptidoglycan layer with hard polysaccharide chains linked by peptides. The thick outer cell wall could hinder NP penetration into the thick peptidoglycan layer [50]. It is known that, in an aerobic environment, pure aluminium reacts with oxygen and forms a thin oxide layer on its surface [51]. Factors that may be responsible for the antibacterial effect of aluminium oxide are (i) zeta potential and size of nanoparticles and (ii) formation of reactive oxidizing species (ROS) [52,53].

4. Conclusions

- (1) The Al NP nanocomposite was successfully dispersed in the epoxy resin and epoxy paint, without agglomerates and the appearance of air bubbles, which was confirmed by SEM, EDS, and SECM analyses.
- (2) Electrochemical tests confirm that the addition of Al NPs to the epoxy paints significantly increases the impedance values. The enhanced corrosion protection performance in the presence of spherical Al NPs was attributed to the cathodic passivation process. After a longer exposure time, oxides form on the Al NP surface, close the pores, and provide greater resistance to the aggressive medium. When the added content of Al NPs was 1.0 wt.%, the nanocomposite displayed the best mechanical and corrosion protection properties.
- (3) The tests of antimicrobial properties against two typical bacteria of *P. aeruginosa* and *B. subtilis* indicate that the surface antibacterial layer of Al NPs possesses excellent antimicrobial properties.
- (4) According to the obtained results, we believe that this Al NP–epoxy nanocomposite represents a multifunctional coating with excellent anticorrosive and antibacterial properties.

Author Contributions: Conceptualization, V.A. and M.S.; methodology, M.S. and M.V.D.; software, M.S. and M.K.; validation, M.S. and M.K.; formal analysis, M.S. and M.K.; investigation, M.S.; resources, V.A.; data curation, M.S.; writing—original draft preparation, M.S.; writing—review and editing, M.S.; visualization, M.S., M.K., M.V.D. and V.A.; supervision, V.A.; project administration, V.A. and M.K.; funding acquisition, V.A. All authors have read and agreed to the published version of the manuscript.

Funding: This research was funded by “Development of anticorrosion protection system for multipurpose pipe use”, grant number KK.01.1.1.07.0045. This work was supported by the European Regional Development Fund under the Operational Program Competitiveness and Cohesion 2014–2020.

Institutional Review Board Statement: Not applicable.

Informed Consent Statement: Not applicable.

Data Availability Statement: Not applicable.

Conflicts of Interest: The authors declare no conflict of interest.

References

1. Melchers, R.E. Post-perforation external corrosion of cast iron pressurised water mains. *Corros. Eng. Sci. Technol.* **2017**, *52*, 541–546. [[CrossRef](#)]
2. Heikh, A.H.; Sarkar, A.; Singh, J.K.; Sohail, M.A.K.; Alharthi, N.; Ghosh, M. Corrosion Characteristics of Copper-Added Austempered Gray Cast Iron (AGCI). *Materials* **2019**, *12*, 503.
3. Umoren, S.A.; Solomon, M.M. Recent Developments on the Use of Polymers as Corrosion Inhibitors—A Review. *Open Mater. Sci. J.* **2014**, *8*, 39–54. [[CrossRef](#)]
4. Jain, P.; Patidar, B.; Bhawsar, J. Potential of Nanoparticles as a Corrosion Inhibitor: A Review. *J. Bio-Tribo-Corros.* **2020**, *6*, 1–12. [[CrossRef](#)]

5. Koch, G.; Varney, J.; Thompson, N.; Moghissi, O.; Gould, M.; Payer, J. International Measures of Prevention, Application, and Economics of Corrosion Technologies Study. *NACE Int.* **2016**, *2016*, 2–3.
6. Koch, G.H.; Brongers, M.P.H.; Thompson, N.G.; Virmani, Y.P.; Payer, J.H. Cost of Corrosion Study Unveiled. *NACE Int.* **2015**, 95–126.
7. Kania, H. Corrosion and Anticorrosion of Alloys/Metals: The Important Global Issue. *Coatings* **2023**, *13*, 216. [[CrossRef](#)]
8. Ferreira, E.S.; Giacomelli, C.; Giacomelli, F.C.; Spinelli, A. Evaluation of the inhibitor effect of L-ascorbic acid on the corrosion of mild steel. *Mater. Chem. Phys.* **2004**, *83*, 129–134. [[CrossRef](#)]
9. Ammar, A.U.; Shahid, M.; Ahmed, M.K.; Khan, M.; Khalid, A.; Khan, Z.A. Electrochemical study of polymer and ceramic-based nanocomposite coatings for corrosion protection of cast iron pipeline. *Materials* **2018**, *11*, 332. [[CrossRef](#)]
10. Foorginezhad, S.; Dargah, M.M.; Firoozirad, K.; Aryai, V.; Razmjou, A.; Abbassi, R.; Garaniya, V.; Beheshti, A.; Asadnia, M. Recent Advances in Sensing and Assessment of Corrosion in Sewage Pipelines. *Process. Saf. Environ. Prot.* **2020**, *147*, 192–213. [[CrossRef](#)]
11. Lv, M.; Du, M. A review: Microbiologically influenced corrosion and the effect of cathodic polarization on typical bacteria. *Rev. Environ. Sci. Biotechnol.* **2018**, *17*, 431–446. [[CrossRef](#)]
12. Slekovec, C.; Plantin, J.; Cholley, P.; Thouverez, M.; Talon, D.; Bartrand, X.; Hocquet, D. Tracking Down Antibiotic-Resistant *Pseudomonas aeruginosa* Isolates in a Wastewater Network. *PLoS ONE* **2012**, *7*, e49300. [[CrossRef](#)] [[PubMed](#)]
13. Perelomov, L.; Sizova, O.; Rahman, M.M.; Perelomova, I.; Minkina, T.; Sokolov, S.; Atroshchenko, Y. Metal-Tolerant Bacteria of Wastewater Treatment Plant in a Large City. *Sustainability* **2022**, *14*, 11335. [[CrossRef](#)]
14. Cyprowski, M.; Stobnicka-Kupiec, A.; Lawniczek-Walczyk, A.; Bakal-Kijek, A.; Gołofit-Szymczak, M.; Górný, R.L. Anaerobic bacteria in wastewater treatment plant. *Int. Arch. Occup. Environ. Health* **2018**, *91*, 571–579. [[CrossRef](#)]
15. Roulová, N.; Mot'ková, P.; Brožková, I.; Pejchalová, M. Antibiotic resistance of *Pseudomonas aeruginosa* isolated from hospital wastewater in the Czech Republic. *J. Water Health* **2022**, *20*, 692–701. [[CrossRef](#)] [[PubMed](#)]
16. Zhao, X.; Yan, L.; Xu, X.; Zhao, H.; Lu, Y.; Wang, Y.; Jiang, C.; Shao, D.; Zhu, J.; Shi, J. Synthesis of silver nanoparticles and its contribution to the capability of *Bacillus subtilis* to deal with polluted waters. *Appl. Microbiol. Biotechnol.* **2019**, *103*, 6319–6332. [[CrossRef](#)]
17. Balakrishnan, A.; Jena, G.; Pongachira George, R.; Philip, J. Polydimethylsiloxane–graphene oxide nanocomposite coatings with improved anti-corrosion and anti-biofouling properties. *Environ. Sci. Pollut. Res.* **2021**, *28*, 7404–7422. [[CrossRef](#)] [[PubMed](#)]
18. Saravanan, P.; Jayamoorthy, K.; Ananda Kumar, S. Design and characterization of non-toxic nano-hybrid coatings for corrosion and fouling resistance. *J. Sci. Adv. Mater. Devices* **2016**, *1*, 367–378. [[CrossRef](#)]
19. Bertani, R.; Bartolozzi, A.; Pontefisso, A.; Quaresimin, M.; Zappalorto, M. Improving the antimicrobial and mechanical properties of epoxy resins via nanomodification: An overview. *Molecules* **2021**, *26*, 5426. [[CrossRef](#)]
20. Yuan, H.; Qi, F.; Zhao, N.; Wan, P.; Zhang, B.; Xiong, H.; Liao, B.; Ouyang, X. Graphene oxide decorated with titanium nanoparticles to reinforce the anti-corrosion performance of epoxy coating. *Coatings* **2020**, *10*, 129. [[CrossRef](#)]
21. Manjumeena, R.; Venkatesan, R.; Duraibabu, D.; Sudha, J.; Rajendran, N.; Kalaichelvan, P.T. Green Nanosilver as Reinforcing Eco-Friendly Additive to Epoxy Coating for Augmented Anticorrosive and Antimicrobial Behavior. *Silicon* **2016**, *8*, 277–298. [[CrossRef](#)]
22. Talabi, H.K.; Adewuyi, B.O.; Olaniran, O.; Ayekusibe, P.O. Reinforcement Efficiency of Copper Nanoparticles on Epoxy Matrix Bactericide Composite. *J. Chem. Technol. Metall.* **2021**, *56*, 321–326.
23. Jamkhande, P.G.; Ghule, N.W.; Bamer, A.H.; Kalaskar, M.G. Metal nanoparticles synthesis: An overview on methods of preparation, advantages and disadvantages, and applications. *J. Drug Deliv. Sci. Technol.* **2019**, *53*, 101174. [[CrossRef](#)]
24. Samardžija, M.; Alar, V.; Špada, V.; Stojanović, I. Corrosion Behaviour of an Epoxy Resin Reinforced with Aluminium Nanoparticles. *Coatings* **2022**, *12*, 1500. [[CrossRef](#)]
25. *Aalco Aluminium Alloy Specifications Datasheet*; Aalco Metals Ltd.: Wednesbury, UK, 2016; pp. 1–6.
26. Pesiri, D.; Aumann, C.; Bilger, L.; Booth, D.; Carpenter, R.D.; Dxe, R.; O'Neill, E.; Shelton, D.; Walter, K.C. Industrial scale nano-aluminum powder manufacturing. *J. Pyro.* **2007**, *714*, 1–16.
27. Kumar, A.M.; Khan, A.; Suleiman, R.; Qamar, M.; Saravanan, S.; Dafalla, H. Bifunctional CuO/TiO₂ nanocomposite as nanofiller for improved corrosion resistance and antibacterial protection. *Prog. Org. Coatings* **2017**, *114*, 9–18. [[CrossRef](#)]
28. *ISO 868*; Plastic and Ebonite—Determination of Indentation Hardness by Means of a Durometer (Shore Hardness). International Organization for Standardization: Geneva, Switzerland, 2003.
29. *ISO 6270-2*; Paints and Varnishes—Determination of Resistance to Humidity—Part 2: Condensation (In-Cabinet Exposure with Heated Water Reservoir). International Organization for Standardization: Geneva, Switzerland, 2017.
30. Chaudhary, R.G.; Tanna, J.A.; Gandhare, N.V.; Rai, A.R.; Juneja, H.D. Synthesis of nickel nanoparticles: Microscopic investigation, an efficient catalyst and effective antibacterial activity. *Adv. Mater. Lett.* **2015**, *6*, 990–998. [[CrossRef](#)]
31. *ISO 12944-6*; Paints and Varnishes—Corrosion Protection of Steel Structures by Protective Paint Systems—Part 6: Laboratory Performance Test Methods. International Organization for Standardization: Geneva, Switzerland, 2018.
32. Wei, H.; Xia, J.; Zhou, W.; Zhou, L.; Hussian, G.; Li, Q.; Ostrikov, K.K. Adhesion and cohesion of epoxy-based industrial composite coatings. *Compos. B Eng.* **2020**, *193*, 108035. [[CrossRef](#)]
33. Sherif, E.S.M.; Alam, M.A.; Al-Zahrani, S.M. Fabrication of Different Protective Coatings and Studying their Mechanical Properties and Corrosion Behavior in Sodium Chloride Solutions. *Int. J. Electrochem. Sci.* **2015**, *10*, 373–387.

34. Margarit-Mattos, I.C.P. EIS and organic coatings performance: Revisiting some key points. *Electrochim. Acta* **2020**, *354*, 136725. [[CrossRef](#)]
35. Chilkoor, G.; Sarder, R.; Islam, J.; Kumar, K.E.A.; Ratnayake, I.; Star, S.; Jasthi, B.K.; Sereda, G.; Koratkar, N.; Meyyappan, M.; et al. Maleic anhydride-functionalized graphene nanofillers render epoxy coatings highly resistant to corrosion and microbial attack. *Carbon N. Y.* **2020**, *159*, 586–597. [[CrossRef](#)]
36. Shankar, A.R.; Anandkumar, B.; Thinaharan, C.; George, R.P.; Rooby, J.; Philip, J.; Kamachi Mudali, U. Corrosion Evaluation of Buried Cast Iron Pipes Exposed to Fire Water System for 30 years. *Trans. Indian Inst. Met.* **2020**, *73*, 9–21. [[CrossRef](#)]
37. Liu, X.; Xiong, J.; Lv, Y.; Zuo, Y. Study on corrosion electrochemical behavior of several different coating systems by EIS. *Prog. Org. Coatings* **2009**, *64*, 497–503. [[CrossRef](#)]
38. Dave, P.N.; Chopda, L.V.; Sahu, L. Applications of Nanomaterials in Corrosion Protection Inhibitors and Coatings. *ACS Symp. Ser.* **2022**, *1418*, 189–212.
39. Trentin, A.; Pakseresht, A.; Duran, A.; Castro, Y.; Galusek, D. Electrochemical Characterization of Polymeric Coatings for Corrosion Protection: A Review of Advances and Perspectives. *Polymers* **2022**, *14*, 2306. [[CrossRef](#)]
40. Niroumandrad, S.; Rostami, M.; Ramezanzadeh, B. Effects of combined surface treatments of aluminium nanoparticle on its corrosion resistance before and after inclusion into an epoxy coating. *Prog. Org. Coatings* **2016**, *101*, 486–501. [[CrossRef](#)]
41. Kurtela, M.; Šimunović, V.; Stojanović, I.; Alar, V. Effect of the cerium (III) chloride heptahydrate on the corrosion inhibition of aluminum alloy. *Mater. Corros.* **2019**, *71*, 125–147. [[CrossRef](#)]
42. Chernavskii, P.A.; Peskov, N.V.; Mugtasimov, A.V.; Lunin, V.V. Oxidation of metal nanoparticles: Experiment and model. *Russ. J. Phys. Chem.* **2007**, *1*, 394–411. [[CrossRef](#)]
43. Petrovic, J.; Thomas, G. Reaction of Aluminum with Water to Produce Hydrogen, a Study of Issues Related to the Use of Aluminum for On-Board Vehicular Hydrogen Storage. *U.S. Dep. Energy* **2008**, *1*, 1–26.
44. Gromov, A.A.; Strokova, Y.I.; Teipel, U. Stabilization of metal nanoparticles—A chemical approach. *Chem. Eng. Technol.* **2009**, *32*, 1049–1060. [[CrossRef](#)]
45. Gerard, D.; Gray, S.K. Aluminium plasmonics. *J. Phys. D. Appl. Phys.* **2015**, *48*, 184001. [[CrossRef](#)]
46. Schmidt, R.G.; Bell, J.P. Epoxy Adhesion to Metals. *Adv. Polym.* **1986**, *75*, 33–71.
47. Feichtenschlager, B.; Pabisch, S.; Svehla, J.; Peterlik, H.; Sajjad, M.; Koch, T.; Kickelbick, G. Epoxy Resin Nanocomposites: The Influence of Interface Modification on the Dispersion Structure—A Small-Angle-X-ray-Scattering Study. *Surfaces* **2020**, *3*, 664–682. [[CrossRef](#)]
48. Taylor, P.; Halder, S.; Ghosh, P.K.; Goyat, M.S.; Ray, S. Ultrasonic dual mode mixing and its effect on tensile properties of SiO₂-epoxy nanocomposite. *J. Adhes. Sci. Technol.* **2013**, *27*, 37–41.
49. Xavier, J.R.; Nallaiyan, R. Application of EIS and SECM Studies for Investigation of Anticorrosion Properties of Epoxy Coatings containing ZrO₂ Nanoparticles on Mild Steel in 3.5% NaCl Solution. *J. Fail. Anal. Prev.* **2016**, *16*, 1082–1091. [[CrossRef](#)]
50. Slavin, Y.N.; Asnis, J.; Häfeli, U.O.; Bach, H. Metal nanoparticles: Understanding the mechanisms behind antibacterial activity. *J. Nanobiotechnol.* **2017**, *15*, 1–20. [[CrossRef](#)]
51. Karlsson, P.; Palmqvist, A.E.C.; Holmberg, K. Surface modification for aluminium pigment inhibition. *Adv. Colloid Interface Sci.* **2006**, *128–130*, 121–134. [[CrossRef](#)]
52. Prashanth, P.A.; Raveendra, R.S.; Krishan, R.H.; Ananda, S.; Bhagya, N.P.; Nagabhushana, B.M. Synthesis, characterizations, antibacterial and photoluminescence studies of solution combustion-derived α -Al₂O₃ nanoparticles. *J. Asian Ceram. Soc.* **2015**, *3*, 345–351. [[CrossRef](#)]
53. Gudkov, S.V.; Burmistrov, D.E.; Smirnova, V.V.; Semenova, A.A.; Lisitsyn, A.B. A Mini Review of Antibacterial Properties of Al₂O₃ Nanoparticles. *Nanomaterials* **2022**, *12*, 2635. [[CrossRef](#)]

Disclaimer/Publisher’s Note: The statements, opinions and data contained in all publications are solely those of the individual author(s) and contributor(s) and not of MDPI and/or the editor(s). MDPI and/or the editor(s) disclaim responsibility for any injury to people or property resulting from any ideas, methods, instructions or products referred to in the content.